Inductor Optimization for Passive Wireless Implantable Capacitive Sensors

by Neel Shah

Research Project

Submitted to the Department of Electrical Engineering and Computer Sciences, University of California at Berkeley, in partial satisfaction of the requirements for the degree of **Master of Science, Plan II**.

Approval for the Report and Comprehensive Examination:

Committee:

Professor Shuvo Roy

Research Advisor

(Date)

* * * * * * *

Professor Al Pisano

Second Reader

(Date)

I. INTRODUCTION

There are many clinical scenarios in which continuous monitoring of vital physiological signs is desired. Pressure monitoring in particular has diverse uses in the body. Specific application areas include checking arterial blood pressure for detection of changing heart conditions, monitoring intracranial pressure for stroke victims, tracking post-surgery pressure profiles in spinal columns to determine treatment efficacy, and recording subtle changes in intraocular pressure to detect the onset of glaucoma [1, 2, 3, 4]. Many of these applications are in space-constrained regions of the body that are difficult to access. A sufficiently small implantable solution would address the challenges of obtaining accurate pressure measurements in such inaccessible regions of the body, and a wireless solution would address the challenge of continuous access. Such a device would promote effective intervention and treatment for chronic, pressure-dependent conditions.

For the continuous monitoring of chronic conditions, an implantable device should possess certain features: 1) Implantation should be minimally invasive, 2) its use and operation should not be an encumbrance to physician or patient, and 3) it should operate maintenance-free for several months to years. For minimally invasive procedures it is desirable to maintain an extremely small form factor, on the order of cubic millimeters in volume. An *in vivo* monitoring device should not have any external wires or "wearable" components; instead relying on wireless transmission for readout. Ensuring maintenance-free operation rules out the use of batteries and active elements, and necessitates a low drift sensor.

Based on the above criteria, passive wireless sensor technology is a natural platform for such a device. Passive wireless sensors are realizable in small form factor using micro-fabricated inductors in conjunction with MEMS capacitive sensors, thus allowing for minimally invasive implantation. This setup uses an inductive coil for wireless power transfer, thus eliminating any external leads. The combination of the inductor and variable capacitor circuit creates a resonant tank whose resonant frequency is dependent on the sensed value, thus creating a maintenance-free, battery-less sensing system. This device can be encased in a biocompatible material to ensure long-term operation.

Prior works have implemented this design paradigm to produce implantable wireless pressure sensors, but have yielded devices that are too large for certain clinical applications, such as spinal pressure monitoring [5, 6]. Implantable wireless sensors typically operate at resonance in the low frequency domain for efficient through-body power transfer [7], which necessitates the use of large inductance or capacitance values that require large areas. However, inductors with small areas have lower power transfer due to smaller flux, which reduces signal-to-noise ratio and makes read-out more difficult. Hence, an optimization is necessary to balance the needs of small size and low frequency while maximizing the device response to external signals for robust and reliable communication.

Unfortunately, most literature on LC tank design optimization is geared towards off-resonance filtering, or high-frequency power matching, which is unsuitable for low-frequency on-resonance use [8, 9]. While simulation software does exist to predict device performance in this regime, they tend to be laborious; optimizing device geometry requires an extremely long time [10, 11]. Fabrication and measurement of devices is possible and fairly simple, but this method has a long turn-around time and is costly. Thus there exists a need for fast analytic design and subsequent optimization of inductor geometry for use in low-frequency resonant tanks.

In this work, a quick turn-around design methodology is developed for planar inductors to be used in the low frequency magnetic coupling regime. A parameterized model is employed for planar inductive coils coupled with sensor capacitors. Designs are optimized with clinical, fabrication and operational constraints in mind. Calculations are compared to simulations and measurements of such devices, and the models are refined to improve agreement.

II. BACKGROUND

The circuit paradigm for the passive sensor is an LC tank, as shown in Figure 1 (left). The lumped element model for an inductor includes series resistance (R) and self-capacitance (C) that when placed in series with a capacitive sensor (C_S, modeled here as an ideal capacitor) forms an RLC circuit with resonant frequency and quality factor:

$$f_0 = \left(2\pi\sqrt{L(C + C_s)}\right)^{-1} \quad (1)$$

$$Q = R^{-1}\sqrt{L(C + C_S)^{-1}} \quad (2)$$

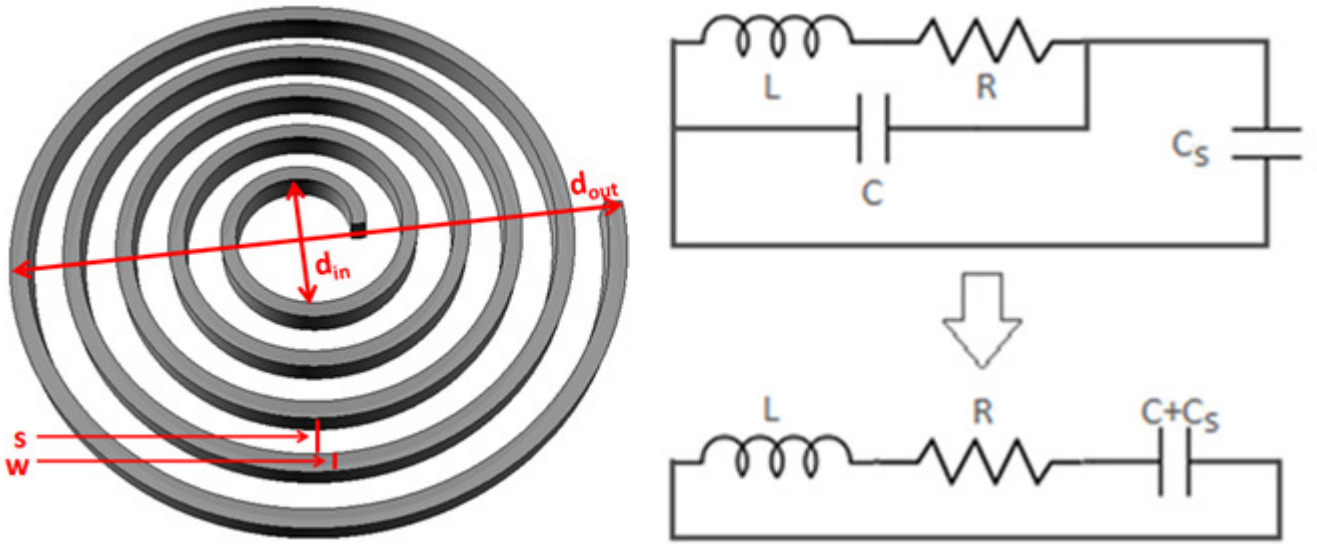

Figure 1: (left) Physical layout and parameters of planar inductor. (right) Circuit diagram and simplification.

Prior work has established analytical models for planar inductors based on geometric parameters [12, 13]. A circular coil can be completely defined by the trace width (w), the trace spacing (s), the number of turns (N), and the outer diameter (d_{out}). An analytical approximation for inductance based on these parameters is

$$L = \frac{1}{4}\mu_0 N^2 (d_{in} + d_{out})\left[\ln\frac{2.46}{p} + 0.20p^2\right] \quad (3)$$

where d_{in} is the inner diameter of the coil and p is the fill factor, which are defined as

$$d_{in} = d_{out} - (2N + 1)w - (2N - 1)s \quad (4)$$

$$p = (d_{out} - d_{in})/(d_{out} + d_{in}) \quad (5)$$

The 1σ error for this inductance approximation is about 6-7% [12].

The self-capacitance of a planar inductor is typically dominated by the underpass capacitance, which is determined by the thickness and permittivity of the separation layer [13]:

$$C = \epsilon_{ox} N w^2 / t_{ox} + C_{interwinding} \approx \epsilon_{ox} N w^2 / t_{ox} \quad (6)$$

The resistance of the coil is frequency dependent due to the skin effect and is approximated as:

$$R = R_{DC} \cdot \frac{T}{\delta} \cdot \frac{1}{1 - e^{-T/\delta}} = \frac{l}{\sigma w \delta (1 - e^{-T/\delta})} \quad (7)$$

Where δ is the frequency-dependent skin depth, T is the coil thickness, σ is the conductivity of the coil and l is the coil length. The formula for Archimedean spirals is used to calculate the coil length [14]:

$$l = \frac{w + s}{4\pi}\left[4\pi^2\left(N^2 + \frac{N d_{in}}{w + s}\right) + \ln\left(1 + \frac{2N(w + s)}{d_{in}}\right)\right] \quad (8)$$

III. METHODS

A. Analytical Optimization

For a given inductor design and sensor capacitor C_S, the device resonant frequency and quality factor can be determined by equations (1) and (2). Conversely, given constraints for resonant frequency and size the necessary geometric parameters can be determined for optimal quality factor. Quality factor is optimized for specifically to maximize the sensitivity of resonant frequency to sensed pressure. To accomplish this, the clinical, fabrication, and operational constraints are translated into design constraints, which are then used in a standard global optimization framework [15].

The key clinical constraint is the minimally invasive implantation, which limits the outer diameter of the device depending on specific application. For eye and spinal implants we assume $d_{MAX} = 2\ mm$ and $d_{MAX} = 4\ mm$.

The fabrication constraints limit the minimum feature size and aspect ratio for the geometry and maximum metal thickness. The thickness is set to the maximum possible as it maximizes quality factor without impacting frequency or size. For millimeter scale circular coils, the maximum reliable aspect ratio is 3:1; this sets the minimum feature size (trace width and spacing) to $w_{MIN} = s_{MIN} = 10\ \mu m$.

The operational constraint limits the maximum frequency of operation. Power transfer through tissue is most efficient at low frequencies due to the Debye relaxation loss [16]. Hence, the operation frequency is limited to $f_{MAX} = 50\ MHz$. Following RF design rules, the metal thickness is set to $T_{MAX} = 30\ \mu m$ to capture at least 3 skin depths. The lumped element modeling approach also requires the coil length to be less than $\lambda/10$, where λ is the wavelength of operation.

The constraints and design equations are summarized in a monotonicity table as shown below [15]. Our design variables are trace width (w), trace spacing (s), number of turns (N), and outer diameter (d_{out}), which creates a four-dimensional design space. Using monotonic analysis, an attempt is made to reduce the design space dimensions and thus reduce computational complexity. All unshaded rows indicate constraints which actively constrain the optimal solution. In contrast, the shaded rows indicate constraints which are neither active nor relevant.

#	Equation	w	s	N	d_{out}	f_0	l	d_{in}	p	L	R	C
Obj	$Q^{-1} = R\sqrt{(C + C_s)/L}$									-	+	+
G1	$d_{out} - d_{MAX} \leq 0$				+							
G2	$w_{MIN} - w \leq 0$	-										
G3	$s_{MIN} - s \leq 0$		-									
G4	$f_0 - f_{MAX} \leq 0$					+						
G5	$l - l_{MAX} \leq 0$						+					
G6	$d_{MIN} - d_{in} \leq 0$							-				
H1	$d_{in} - d_{in}(w, s, N, d_{out}) = 0$	-	-	-	+			-				
H2	$l - l(w, s, N, r_{in}) = 0$	+	+	+			-	+				
H3	$p - p(w, s, N, d_{out}) = 0$	+	+	+	-				-			
H4	$L - L(w, s, N, d_{out}, p) = 0$	-	-	-	-				+	+		
H5	$R - R(w, l) = 0$	-					+				-	
H6	$C - C(w, N) = 0$	?		?								??
H7	$f_0 - f_0(L, C) = 0$					-				-		-

Table 1: Monotonicity analysis for inductor optimization. The objective function to minimize is the inverse of quality factor. Plus and minus symbols represent the sign of each variable (columns) in each equation (rows). Equations are constructed by placing equalities (Hx) and inequalities (Gx) in canonical form. Complex equality constraints are represented abstractly as functions.

It can be shown that quality factor monotonically increases with respect to outer diameter. Substituting for inner diameter in equation (5), it can be seen that fill ratio decreases as outer diameter increases:

$$p = \frac{d_{out} - d_{in}}{d_{out} + d_{in}} = \frac{(2N+1)w + (2N-1)s}{2d_{out} - (2N+1)w - (2N-1)s} \tag{9}$$

As d_{out} increases, p decreases below 1, and the inductance increases exponentially due to the $-\ln p$ term. Thus inductance increases exponentially with respect to outer diameter. Increasing outer diameter also increases the resistance by affecting the length; however this relationship is only linear, and **the net effect is a monotonic increase of Q with respect to outer diameter**.

It can also be shown that quality factor monotonically decreases with respect to spacing. The fill ratio always increases as trace spacing increases, and the derivative is always greater than zero:

$$\frac{\partial p}{\partial s} = \frac{2d_{out}(2N-1)}{(2d_{out} - (2N+1)w - (2N-1)s)^2} \tag{10}$$

The inductance does have a positive linear term in s, but again the $-\ln p$ term dominates and an exponential decrease in L results. Similarly there exists in resistance a linear dependence on s; since L drops and R rises as s rises, Q always drops, and **thus Q monotonically decreases with respect to spacing.**

It is important to note that the inner diameter d_{in} does not monotonically increase with respect to coil length, i.e. there is a stationary point below which length decreases. Taking the derivative of length with respect to inner diameter:

$$\frac{\partial l}{\partial d_{in}} = 2\pi N + \frac{N(w+s)^2/2\pi}{2N(w+s)d_{in} + d_{in}^2} \therefore d_{in,crit} = \frac{w+s}{4\pi^2 N} \tag{11}$$

The maximum possible value $d_{in,crit}$ can take on (when $N = 1,\ w = 100\ \mu m$) is 2.8 μm, which is far below a reasonable d_{in} for the design space. Thus it is fair to state length increases monotonically with respect to inner diameter.

Since Q increases with respect to diameter and decreases with respect to spacing, those variables can be fixed to their limits. That is, the outer diameter is fixed to the maximum and the trace spacing is fixed to the minimum. There now remain two free design parameters N and w. A sweep over our constrained parameter space (now only 2 dimensions) can find which values of w and N yield the optimal quality factor design that satisfies coil length and resonant frequency constraints. MATLAB code is developed to generate coils with the presented parameterization and calculate its circuit parameters and quality factor. The code disregards coils that violate the length and frequency constraints.

For our proposed sensor applications where wireless monitoring of ocular and spinal pressure is desired, 2 and 4 mm outer diameter coils are optimized and parameterized. In addition, 6 mm outer-diameter coils are processed as a larger reference design. External C_S capacitors in the 1-20 pF range are chosen to keep resonant frequency under 50 MHz.

B. Field Solver Verification

The optimal device geometries were simulated in Sonnet EM simulation software using a one port measurement setup spanning the frequency range 1 to 100 MHz [10]. The coil geometry was simulated with an ideal capacitor representing the capacitive sensor. A 9 μm x 9 μm cell size was set to minimize simulation time while still avoiding virtual shorts between coil turns. A thin metal model was used for the coil, which simulates skin effects but not interwinding capacitance. The dielectric stack used reflects the layers generally utilized in MEMS device fabrication. The coil was simulated in a 1.25 x 1.25 cm^2 area, with 1 cm of air above and below the device. A 2 micron oxide spacer separates the top coil layer from the bottom underpass, which rests on a 0.5 mm glass substrate. The measurement setup is a series RLC circuit, so minimum impedance is expected at the resonant frequency. Sonnet calculates the input impedance and converts to dB using a $20 \cdot \log_{10} Z$ scale; thus the quality factor can be extracted from the 3 dB bandwidth of the impedance trace. As an additional level of verification, the RLC circuit parameters of the inductive coil were also extracted from Sonnet simulations and compared to calculated and measured values. In order to do so, the ideal capacitor was removed from the circuit and the coil was re-simulated to obtain the resistance and inductance values. The coil self-capacitance was determined from the self-resonant frequency.

C. Experimental Verification

The designs were micro-fabricated and tested with a wireless probe for validation. Figure 2 shows the top-view and schematic cross-section of a fabricated device. The inductor was fabricated on a 500 µm thick glass substrate to avoid significant substrate losses seen in inductors on silicon [17]. A 0.5 µm thick Cr/Au layer was deposited and patterned to form the coil underpass and bottom capacitor plate. A 2 µm of silicon oxide film was deposited, patterned, and etched to expose the end of the underpass. Finally, the coils and upper capacitor plates were formed using a photoresist mold and a 30 µm thick electroplated copper layer.

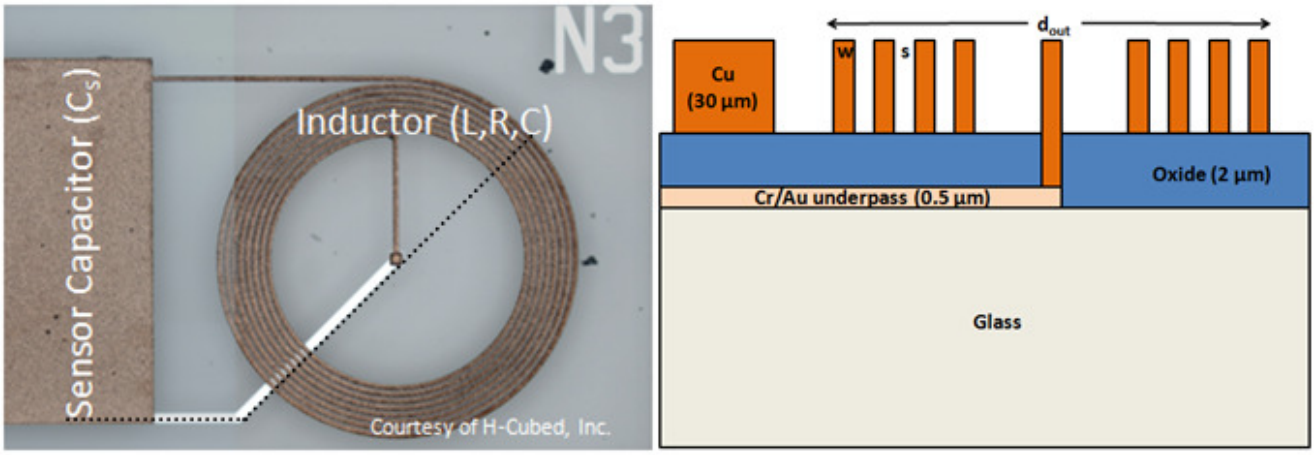

Figure 2: (left) Device layout. (right) Device stackup (cross-section shown in left)

Testing was performed using an orthogonal coil probe to wireless drive and sense the response from fabricated coils [18]. This probe minimizes interference between the coil transmitting power to the implanted sensor and the coil reading the sensor's resonant response. The probe can also be tuned to minimize the local noise floor to the peak requiring examination. The coil was placed flat and face up on the shell covering of the probe, which stands 1 cm apart from the orthogonal coils inside. The output was monitored on an Agilent E5061B network analyzer. With the transmit coil acting as port 1 and the receive coil reading the sensor response as port 2, resonant frequency and quality factor were obtained from S_{21} measurements.

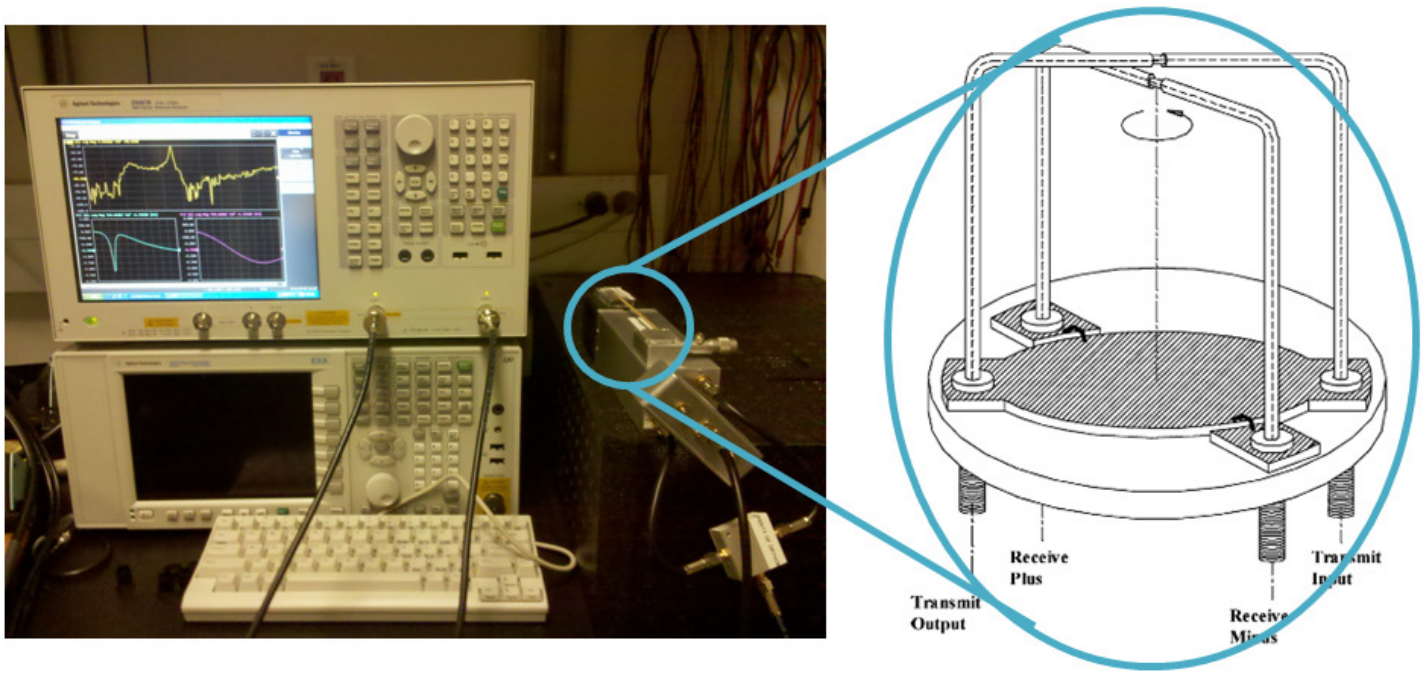

Figure 3: Test setup. Orthogonal coil probe expanded and shown to right. [12]

D. Optimization Verification

To verify the optimization algorithm produces the highest Q device, a design of experiments approach was implemented. 4mm coils in the (w, N) parameter space around the optimal design were fabricated and their frequencies and Q-factors were measured.

Due to difficulties in fabrication the copper conductance was measured to be far lower than the expected value used in the optimization equations. The actual conductance was measured and the calculations were re-run to obtain corrected coil quality factors for better comparison to measured quality factors.

IV. RESULTS

A. Optimization

The MATLAB code output the following optimal designs and parameters for coil diameters of 2 mm, 4 mm, and 6 mm.

	w (µm)	s (µm)	N	d_{out} (mm)	R	L (µH)	C (pF)	Cs (pF)	f_0 (MHz)	Q
2-opt	42	10	14	2	3.35	0.23	0.43	40.0	52.08	22.5
4-opt	61	10	21	4	6.34	1.01	1.35	9.7	47.65	48.1
6-opt	75	10	27	6	8.77	2.42	2.62	5.0	37.09	64.2

Table 2: Analytical optimization results.

B. Simulation

The simulation results are summarized in Table 3, with sample impedance curve shown to the right. The deviation between calculations and simulations is within 2% for the 4 mm optimal coil. For the smaller 2 mm coil higher error in Q prediction is observed; for the larger 6mm coil higher error in resonant frequency prediction is observed.

Design	Calculated Values		Simulated Values		Error	
	f_0 (MHz)	Q	f_0 (MHz)	Q	F0	Q
2-opt	52.1	22.5	50.1	19.7	+3.8 %	+ 12.4 %
4-opt	47.7	48.1	48.7	48.7	- 2.1 %	- 1.2 %
6-opt	37.1	64.2	42.2	60.3	- 12.1 %	+ 6.0 %

Table 3: Simulation results of optimally generated designs.

The simulated circuit parameters were then compared to values calculated by the MATLAB code. The runtime of the MATLAB calculations are orders of magnitude faster than simulation of the same design.

Design	Calculated Values			
	R (Ω)	L (µH)	C (pF)	Runtime
2-opt	3.35	0.23	0.43	66 ms
4-opt	6.34	1.01	1.35	9 ms
6-opt	8.76	2.42	2.62	8 ms

	Simulated Values			
	R (Ω)	L (µH)	C (pF)	Runtime
2-opt	4.11	0.25	0.30	32 minutes
4-opt	7.73	1.07	0.63	11 hours
6-opt	12.1	2.40	1.05	1.5 days

	Calculation Error w.r.to Simulation			
	R (Ω)	L (µH)	C (pF)	Runtime
2-opt	-18%	-8%	43%	N/A
4-opt	-18%	-6%	114%	N/A
6-opt	-28%	1%	150%	N/A

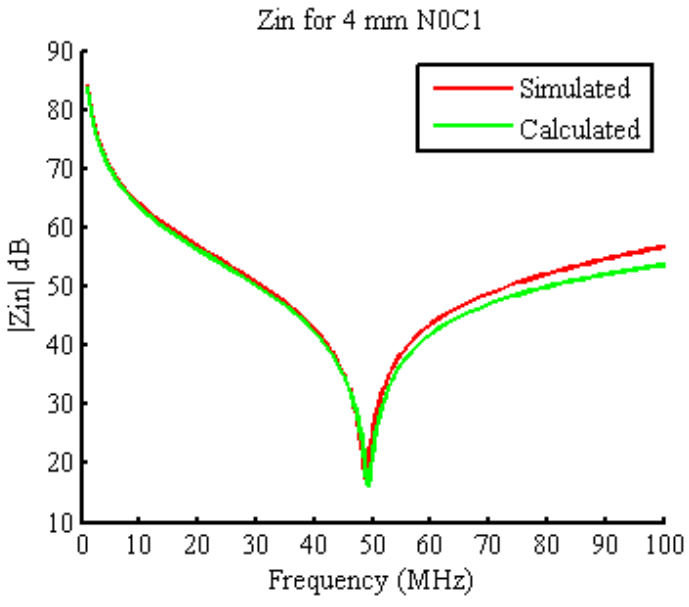

Table 4: (left) Comparison between calculated and simulated circuit parameters. (right) Impedance comparison for 4mm optimal design.

C. Measurement

The resonant frequency calculations are within 2% of measured values. However the calculated Q-values are roughly 2.5 times higher than measured values. Wireless measurements of 2mm coils proved to be not possible due to low SNR. Table 5 displays the data on the left with a sample S_{21} response to the right.

Design	Calculated Values	
	f_0 (MHz)	Q
2-opt	52.1	22.5
4-opt	47.7	48.1
6-opt	37.1	64.2

	Avg. Measured Values		
	f_0 (MHz)	Q	# Tested
2-opt	N/A	N/A	N/A
4-opt	47.0	19.6	2
6-opt	37.5	24.2	4

	Error vs. Measurement	
	f_0	Q
2-opt	N/A	N/A
4-opt	+ 1.5 %	+ 145 %
6-opt	+ 1.1 %	+ 165 %

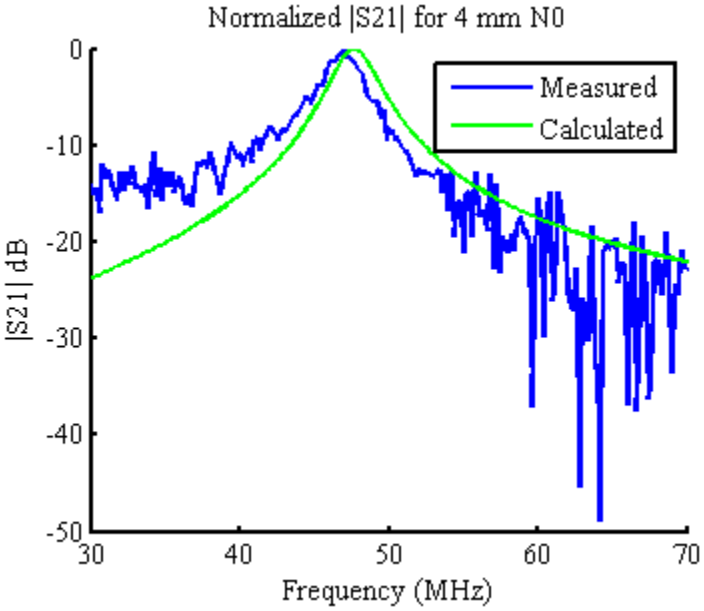

Table 5: (left) Comparison between calculated and measured operating parameters. (right) Forward voltage gain for 4 mm optimal design.

D. Optimization Verification

Table 6 below compares the simulations and calculations for all 4 mm coils as compared to the optimal 4 mm design.

Design	w (µm)	s (µm)	N	dout (mm)	Cs (pF)	Calculated Values		Simulated Values		Error	
						f_0 (MHz)	Q	f_0 (MHz)	Q	f_0	Q
4-opt	61	10	21	4	9.7	47.7	48.1	48.7	48.7	-2.1%	-1.2%
4N1	38	10	11	4	15.1	47.7	31.7	46.3	30.9	3.0%	2.6%
4N2	66	10	11	4	21.6	46.4	41.0	45.5	37.9	2.0%	8.2%
4N3	51	10	17	4	10.8	45.9	43.8	45.6	45.6	0.7%	-3.9%
4N4	38	10	23	4	6.5	44.6	42.6	44.6	49.5	0.0%	-13.9%
4N5	66	10	23	4	12.9	43.3	44.3	44.6	34.2	-2.9%	29.5%

Table 6: Comparison between calculated and simulated results of 4 mm coils. Calculated Q values use ideal copper conductance.

A more realistic conductance value was found by taking coil DC resistance measurements. The average measured conductance was found to be 20.7 ± 2.5 MS/m, which is 30-38% of the ideal value used ($\sigma_{Cu} = 59.6\ MS/m$). Re-running the optimization code with the measured copper conductance yielded the following comparison with respect to measured values.

Design	w (μm)	s (μm)	N	dout (mm)	Cs (pF)	Calculated Values		Avg. Measured Values			Error	
						f_0 (MHz)	Q	f_0 (MHz)	Q	# Tested	f_0	Q
4-opt	61	10	21	4	9.7	47.7	21.9	47.0	19.6	2	1.5%	11.7%
4N1	38	10	11	4	15.1	47.7	14.8	44.9	16.0	2	6.2%	-7.5%
4N2	66	10	11	4	21.6	46.4	18.7	46.7	17.1	2	-0.6%	9.4%
4N3	51	10	17	4	10.8	45.9	20.1	43.7	19.0	3	5.0%	5.8%
4N4	38	10	23	4	6.5	44.6	19.6	41.9	21.8	3	6.4%	-10.1%
4N5	66	10	23	4	12.9	43.3	19.8	43.6	14.5	1	-0.7%	36.6%

Table 7: Comparison between calculated and measured results of 4mm coils. Calculated Q values use measured copper conductance.

The average error in predicting resonant frequency versus simulation is 1.78%; versus measurement it is 3.4%. The average error in predicting quality factors versus simulation is 9.9%; versus measurement it is around 13.5%.

Running the optimization code with the new copper conductance also yielded a new optimal design with more turns and less trace width.

Design	w (μm)	s (μm)	N	d_{out} (mm)	R	L (μH)	C (pF)	Cs (pF)	f_0 (MHz)	Q
4-new	54	10	23	4	17.07	1.24	1.16	7.0	50.0	22.8

Table 8: New 4mm optimal design with more turns and less trace width.

V. DISCUSSION

Simulations of the 4 mm designs yield resonant frequencies and quality factors within the expected bounds of the calculations. The calculations yield resonant frequencies that are in some instances closer to the measured values than simulation. Despite the error inherent to the calculation, the tradeoff in execution time makes the approximations worthwhile for applications requiring first-order solutions.

The simulated inductances of the coils align very closely with calculations, to within 8%. The simulated resistance is however higher, and the simulated capacitance is much lower. This is most prominent in the 6mm coil, where the simulated coil self-capacitance is so low as to drastically change the simulated resonant frequency. However it is noted that for this point that the measured values for the coil match the calculations much more closely than the simulations. This indicates the capacitance modeling equation used for RF inductors is not a good match for inductors in this application.

The low SNR of the 2 mm coils could be due to the poor conductivity of the fabricated coils, which pushes the device quality factor so low such that it cannot be wirelessly measured. It could also be due to the small area of the inductor not being able to pickup and re-radiate enough energy to be detected by the orthogonal coil probe. This would hint towards another tradeoff between coil size and power coupling, which will be explored further in future work. This can also hint at a possible explanation for the 4N4 design having a higher quality factor than the 4N0 design. Since it has a much larger fill ratio p it is perhaps capable of picking up and re-radiating more energy that can be detected by the external probe.

For resonant frequency we find a low degree of error between calculations and measurements. As stated above, the current sheet approximation for inductance carries with it a 6-7% error, which roughly converts to a 3-4% error in resonant frequency. One of the measurements falls outside these bounds as shown in Figure 4. This is also implied by the p-test, due to the problem with capacitance modeling stated above.

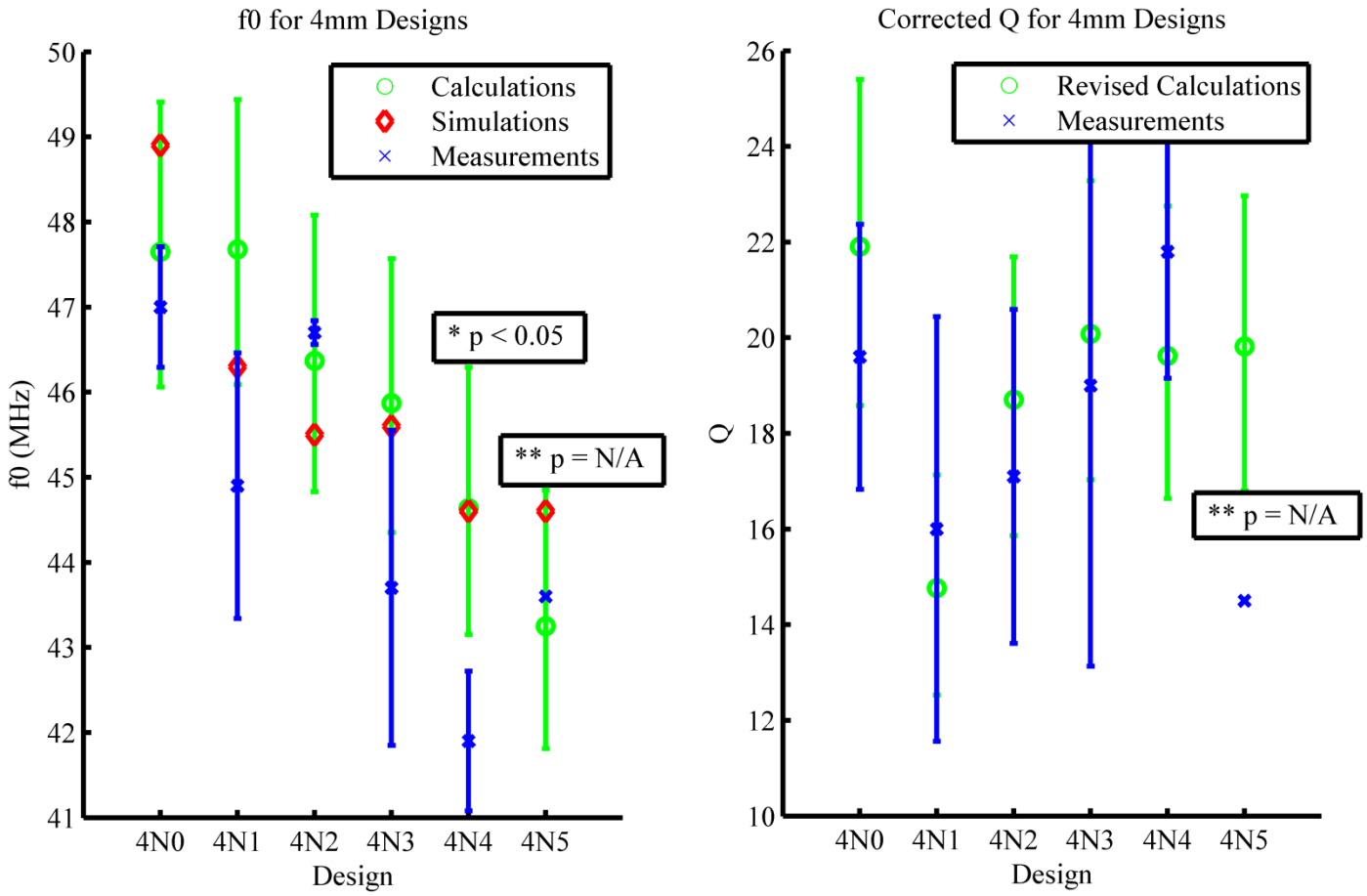

Figure 4: (left) Resonant frequency and (right) quality factor comparisons between calculations, simulations, and measurements, with mean and 1σ error bars shown for calculations and measurements. *4N4 t-test yields a statistically significant difference between resonant frequency measurements and calculations. **Not enough 4N5 samples to run a t-test.

Once the correction for non-ideal coil conductance is applied, it can be seen that the calculations predict the measured quality factors very closely. Once the measured conductance is included in our calculations, the measured 4mm quality factors fall within the accuracy bounds of the calculations. A chart showing this is in Figure 4 to the right. Other attempts at electroplating copper have also reported such substandard conductivity [19]. The negative effect of electroplating on conductivity can be mitigated with a subsequent low-pressure annealing step, hopefully bringing measurements in line with the ideal values [20]. This will be explored in further work.

The new optimal design generated with the corrected copper conductance is none of the designs fabricated for this study. Conversely none of the designs fabricated and simulated are optimal for the given measured conductance. However it can be seen that the revised optimal design has reduced trace width and increased turns, much like the 4N4 design has reduced trace width and increased turns compared to the current optimal design (4N0).

VI. CONCLUSION

A parameterization of inductive coils has been developed that can be used in optimization schemes to maximize the quality factor of wireless sensors. The analytical models presented work from geometric parameters to accurately predict device inductance, capacitance, and resistance much more quickly than simulation. For low frequency, mm-scale coils, resonant frequency can be predicted to within 3.5%, and quality factor can be predicted to within 13.5%. This work can be used to predict device performance prior to fabrication, and the lumped equivalent model can be inserted in larger circuits to predict overall system performance.

Optimization algorithms have also been developed that can be used to determine ideal inductor geometry for a given size and frequency constraints for any application. Based on the tolerances of the fabrication process the geometry will produce a device with quality factor close to or at the maximum possible Q for the given size and frequency constraints.

For wireless power transfer, there is possibly a tradeoff between size and frequency, and work remains to be done to see what the bounds are on magnetic coupling for small size, low frequency wireless power transfer. The distance of operation is another factor that plays into determining the magnetic coupling. Different implantation targets have different required depths of operation, and it needs to be determined what the bounds on operation depth are at a particular coil size. Finally the effects of implanting inside the body need to be modeled and incorporated into coil design. The electromagnetic properties of tissues vary based on cell type, function, device orientation, and how the tissues are layered. All these factors play into the magnetic coupling parameter, which can be modeled as a lossy transformer [13]. A system-level optimization can be performed with this data to create fully functional devices for in situ pressure measurements based on location in the body.

VII. ACKNOWLEDGEMENTS

Mozziyar Etemadi and Rishi Kant provided extensive guidance and valuable input for the study and this report. OrthoMEMS Inc. provided the orthogonal coil device for use in this research. Dr. Hao Jiang provided useful insight throughout this study. Greg Kinnetz provided valuable support for Sonnet simulations. Ken Goldman helped develop the design of experiment and fabricate the devices. Illya Gordon assisted with test equipment setup and measurement. Thura Lin Naing provided useful guidance for developing the MATLAB optimization scheme. Robert Schneider provided wire bonding facilities for sample preparation.

VIII. REFERENCES

[1] K. Takahata, A. DeHennis, K. D. Wise, and Y. B. Gianchandani, “A wireless microsensor for monitoring flow and pressure in a blood vessel utilizing a dual- inductor antenna stent and two pressure sensors,” in *Proc. 17th IEEE Int. Conf. Microelectromechanical Systems (MEMS),* Jan. 25–29, 2004, pp. 216–219.
[2] L.A. Steiner and P.J.D. Andrews, “Monitoring the injured brain: ICP and CBF,” *British Journal of Anaesthesia,* vol. 97, no. 1, pp. 26-38.
[3] K. Stangel, S. Kolnsberg, D. Hammerschmidt, B. J. Hosticka, H. K. Trieu, and W. Mokwa, “A programmable intraocular CMOS pressure sensor system implant,” *IEEE Journal of Solid-State Circuits,* vol. 36, no. 7, pp. 1094–1100, July 2001.
[4] S. Roy, L. A. Ferrara, A. J. Fleischman, and E. C. Benzel, “Microelectromechanical systems and neurosurgery: a new era in a new millennium,” *Neurosurgery,* vol. 49, p. 779, 2001.
[5] C.C. Collins, “A miniature passive pressure transensor for implanting in the eye,” *IEEE Transactions on Biomedical Engineering,* vol. 14, pp. 74-83, Apr. 1967.
[6] M. Fonseca, M. Allen, D. Stern, J. White, and J. Kroh, “Implantable wireless sensor for pressure measurement within the heart,” U.S. Patent 6855115, February 15, 2005.
[7] A. Christ, T. Samaras, A. Klingenbock, and N. Kuster, “Characterization of the electro-magnetic near-field absorption in layered biological tissue in the frequency range from 30 MHz to 6000 MHz,” *Physics in Medicine and Biology,* vol. 51, pp. 4951-4966, Sept. 2006.
[8] D. Ham and A. Hajimiri, “Concepts and Methods in Optimization of Integrated LC VCOs,” *IEEE Journal of Solid-State Circuits,* vol. 36, no. 6, pp. 896-909, June 2001.
[9] D. Li and Y. Tsividis, “Design Techniques for Automatically Tuned Integrated Gigahertz-Range Active LC Filters,” *IEEE Journal of Solid-State Circuits,* vol. 37, no. 8, pp. 967-977, August 2002.
[10] “*Sonnet 12.6,*” Sonnet Software Inc., North Syracuse, NY, 2005.
[11] “*Advanced Design System 2006A,*” Agilent Technologies Inc., Palo Alto, CA, 2005.
[12] S. Mohan, M. del Mar Hershenson, S. Boyd, and T. Lee, “Simple accurate expressions for planar spiral inductances,” *IEEE Journal of Solid-State Circuits,* vol. 34, pp. 1419-1424, Oct. 1999.
[13] T.H. Lee, *The Design of CMOS Radio-Frequency Integrated Circuits.* Cambridge University Press, 2004.

[14] E.W. Weisstein, "Archimedes' Spiral," *Wolfram Mathworld,* http://mathworld.wolfram.com/ArchimedesSpiral.html
[15] D.J. Wilde, *Globally Optimal Design.* John Wiley and Sons, 1978.
[16] S. Gabriel, R.W. Lau, and C. Gabriel, "The dielectric properties of biological tissues: III. Parametric models for the dielectric spectrum of tissues," *Physics in Medicine and Biology,* vol. 41, pp. 2271-2293, 1996.
[17] C.P. Yue and S.S. Wong, "Physical modeling of spiral inductors on silicon," *IEEE Transactions on Electron Devices,* vol. 47, pp. 560-568, Mar. 2000.
[18] J. Talman, A. Fleischman, and S. Roy, "Orthogonal-coil RF probe for implantable passive sensors," *IEEE Transactions on Biomedical Engineering,* vol. 53, pp. 538-546, Mar. 2006.
[19] T. Uelzen, S. Fandrey, and J. Müller, "Mechanical and electrical properties of electroplated copper for MR-imaging coils," *Microsystem Technologies,* vol. 12, pp. 343-351, 2006.
[20] H. Sun, Z. Liu, J. Zhao, L. Wang, and J. Zhu, "The enhancement of Q-factor of planar spiral inductors with low-temperature annealing," *IEEE Transactions on Electron Devices,* vol. 55, pp. 931-936, Mar. 2008.